Articles

Structure of Arylene-Bridged Polysilsesquioxane Xerogels and Aerogels

Dale W. Schaefer,*,† Greg Beaucage,† Douglas A. Loy,‡ Kenneth J. Shea,§ and J. S. Lin||

Department of Chemical and Materials Engineering, University of Cincinnati, Cincinnati, Ohio, 45221-0012, Polymers and Coating Group, Los Alamos National Laboratory, Los Alamos, New Mexico, 87545, Department of Chemistry, University of California, Irvine, Irvine, California 92717, and Oak Ridge National Laboratory, Oak Ridge, Tennessee 37831

Received October 25, 2003. Revised Manuscript Received January 26, 2004

Arylene-bridged polysilsesquioxanes are an interesting class of porous materials prepared by sol−gel processing of ethoxysilane monomers in which there are two or more trialkoxysilyl groups positioned about an arylene bridging group. The majority of these materials are highly porous with surface areas as high as 1880 m^2/g. In an effort to understand the nature of porosity in these materials, small-angle X-ray and neutron scattering were employed to characterize phenylene-, biphenylene-, and terphenylene-bridged polysilsesquioxanes. Phenylene-bridged polysilsesquioxane xerogels and aerogels were also compared to understand the effect of drying protocol on pore structure. The effect of catalyst concentration is also reported for the base-catalyzed system. In all cases studied here, we find evidence for domains in the nanometer range with distinct fractal character. We associate these domains with porosity rather than microphase separation of organic and inorganic moieties. The nature of this porosity depends on the bridging group in a systematic way, but is only weakly dependent on other synthetic parameters such as catalyst type, catalyst concentration, and drying protocol.

Introduction

Hydrocarbon-bridged polysilsesquioxanes represent an interesting class of highly cross-linked hybrid organic−inorganic polymers.[1−9] These materials are network polymers in which the basic building block is two silicons directly attached to a hydrocarbon bridging group (Figure 1). The remaining three bonds to each *silsesquioxane* silicon are siloxane linkages. By connecting two or more silsesquioxane groups to an organic bridging group, a material with as many as six siloxane linkages (Si−O−Si) per monomer unit can be prepared, as opposed to just four in tetraalkoxy silanes. In addition, by introducing hydrocarbon spacers into the siloxane network, the properties (hydrophobicity, surface area, pore size, ultraviolet−visible absorption, and fluorescence, etc.) can be significantly modified.[7,10−12]

Arylene-bridged polysilsesquioxanes **X-1** through **X-4** were prepared by sol−gel processing of bis(triethoxysily)aryl monomers **1**−**4** (Figure 1) under either acidic or basic conditions. Hydrolysis and condensation rapidly leads to gels at concentrations as low as 0.01 M, more than an order of magnitude lower than is possible with triethoxysilylbenzene. Trifunctional aryl silanes preferentially form as oligosilsesquioxanes rather than gels.[13] At high monomer concentration, however, gels can be prepared from trifunctionals with heating and in the presence of strong base.[14]

* To whom correspondence should be addressed. E-mail: dale.schaefer@uc.edu.
† University of Cincinnati.
‡ Los Alamos National Laboratory.
§ University of California.
|| Oak Ridge National Laboratory, current affiliation University of Tennessee, Knoxville.

(1) Shea, K. J.; Loy, D. A.; Webster, O. W. *Chem. Mater.* **1989**, *1*, 572−4.
(2) Shea, K. J.; Loy, D. A.; Webster, O. W. *Polym. Mater. Sci. Eng.* **1990**, *63*, 281−5.
(3) Loy, D. A.; Shea, K. J.; Russick, E. M. In *Better Ceramics Through Chemistry V*; Hampden-Smith, M. J., Klemperer, W. G., Brinker, C. J., Eds.; Mater. Res. Soc. Symp. Proc. 271, Materials Research Society: Pittsburgh, PA, 1992; pp 699−704.
(4) Small, J. H.; Shea, K. J.; Loy, D. A. *J. Non-Cryst. Solids* **1993**, *160*, 234−46.
(5) Corriu, R. J. P.; Leclercq, D. *Angew. Chem. Int. Ed. Engl.* **1996**, *35*, 1420−36.
(6) Cerveau, G.; Corriu, R. J. P.; Lepeytre, C. *J. Organomet. Chem.* **1997**, *548*, 99−103.
(7) Cerveau, G.; Corriu, R. J. P. *Coord. Chem. Rev.* **1998**, *180*, 1051−71.
(8) Corriu, R. *C. R. Acad. Sci., Ser. Ii Fascicule C: Chim.* **1998**, *1*, 83−89.
(9) Boury, B.; Corriu, R. J. P.; Le Strat, V.; Delord, P.; Nobili, M. *Angew. Chem. Int. Ed.* **1999**, *38*, 3172−5.
(10) Loy, D. A.; Shea, K. J. *Chem. Rev.* **1995**, *95*, 1431−42.
(11) Cerveau, G.; Corriu, R. J. P.; Framery, E. *Chem. Mater.* **2001**, *13*, 3373−88.
(12) Shea, K. J.; Loy, D. A. *MRS Bull.* **2001**, *26*, 368−376.
(13) Voronkov, M. G.; Lavrent'yev, V. I. *Top. Curr. Chem.* **1982**, *102*, 199−236.
(14) Frye, C. L.; Klosowski, J. M. *J. Am. Chem. Soc.* **1971**, *93*, 4599−601.

10.1021/cm0350683 CCC: $27.50
Published on Web 03/18/2004

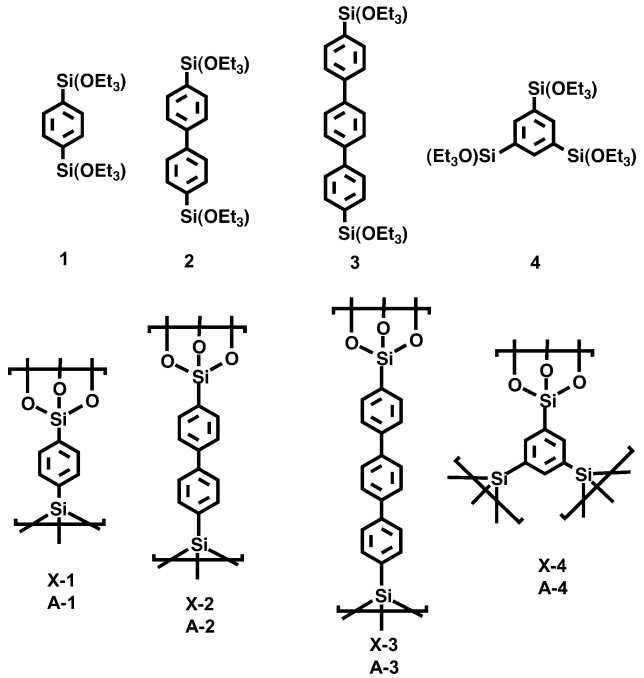

Figure 1. Monomers and reactions: **X-1** is 1,4-phenylene-bridged; **X-2** is 4,4′-biphenylene-bridged; **X-3** is 4,4'-triphenylene-bridged; and **X-4** is 1,3,5-phenylene-bridged. "**X**" refers to a xerogel and "**A**" refers to an aerogel.

Arylene-bridged polysilsesquioxane gels consistently exhibit high surface areas with porosity confined mostly to the nanoporous domain (pore diameters < 20 Å). Surface areas (BET) in phenylene-bridged polysilsesquioxane *xerogels* (air-dried) have been measured by gas porosimetry to be as high as 1200 m^2/g.[15−17] BET surface areas in *aerogels* (supercritically extracted) of the same chemical composition range as high as 1880 m^2/gram.[3]

Bridged polysilsesquioxanes have already been applied for a number of applications including coupling agents for composites,[18] high-surface-area catalytic materials,[19] and protective coatings.[20] These materials have also shown considerable promise as chiral catalysts,[21] metal scavengers,[22−24] chromatographic solid phases, membrane materials,[25] and photonic and electronic materials.[26]

To understand the effect of different arylene bridging groups and synthetic parameters on microstructure, small-angle X-ray (SAXS) and neutron scattering (SANS) experiments were performed. Although scattering cannot provide unambiguous structural information (because of the absence of phase information), these methods are bulk-sensitive and amenable to quantitative interpretation. Moreover, models of pore structure have been developed by interpreting scattering data with the aid of reasonable polymerization schemes, often relying on fractal concepts.[27−29] In all cases studied here, we find evidence for domains in the nanometer range with distinct fractal character. We associate these domains with porosity rather than microphase separation of organic and inorganic moieties. The nature of this porosity depends on the bridging group in a systematic way, but is only weakly dependent on other synthetic parameters such as catalyst type, catalyst concentration, and drying protocol.

Limited SAXS data exist on bridged silsesquioxanes. Schaefer et al.[30] studied the influence of plasma treatment on the evolution of pore morphology in arylene-bridged materials. In this case, only minor changes in pore morphology were observed on elimination of the organic bridges. Boury et al.[31] reported SAXS data on thermally and chemically treated bridged systems. Chemical treatment of a nonporous precursor led to minimal change, whereas thermal treatment produced nanoscale smooth-surface pores. Chevalier et al.[32] studied mixed alkoxy and bridged systems and again observed the development of smooth-surface pores on thermal treatment of nonporous precursors. For the untreated gels, all of these results indicate that there is no phase separation between the organic and inorganic moieties on length scales above 15 Å. Some type of phase separation must occur, however, or the materials would not be porous. It is the purpose of this contribution to understand the nature of this phase separation and how it is controlled by precursor chemistry.

Atomic force microscopy (AFM) and scanning electron microscopy on phenylene-bridged polysilsesquioxane xerogels prepared under both acidic and basic conditions revealed tightly welded aggregates of particles 150−250 Å in diameter. This technique, however, is surface sensitive, possibly obscuring bulk morphology. Using small-angle scattering (SAS) to find domain sizes comparable to that observed with AFM, confirming a relationship between bulk morphology and surface profile.

Gas adsorption has been used extensively to assess the "texture" or surface morphology of bridged hybrids.

(15) Shea, K. J.; Loy, D. A.; Webster, O. *J. Am. Chem. Soc.* **1992**, *114*, 6700−10.
(16) Cerveau, G.; Corriu, R. J. P.; Lepeytre, C.; Mutin, P. H. *J. Mater. Chem.* **1998**, *8*, 2707−13.
(17) Cerveau, G.; Corriu, R. J. P.; Fischmeister-Lepeytre, C. *J. Mater. Chem.* **1999**, *9*, 1149−54.
(18) Kohjiya, S.; Ikeda, Y. *Rubber Chem. Technol.* **2000**, *73*, 534−50.
(19) Brandvold, T. A.; Holmgren, J. S.; Malloy, T. P. U.S. Pat. 5,-475,162; UOP, 1994.
(20) Thurn, F.; Wolff, S. *Kautsch. Gummi. Kunstst.* **1975**, 733.
(21) Hesemann, P.; Moreau, J. J. E. *Tetrahedron: Asymmetry* **2000**, *11*, 2183−94.
(22) Kirillov, A. I.; Panezhda, E. V.; Pozhidaev, Y. N.; Belousova, L. Y.; Vlasova, N. N.; Voronkov, M. G. *Russ. J. Appl. Chem.* **2000**, *73*, 554−5.
(23) Vlasova, N. N.; Kirillov, A. I.; Pozhidaev, Y. N.; Panezhda, E. V.; Belousova, L. I.; Voronkov, M. G. *Dokl. Akad. Nauk* **1999**, *364*, 492−4.
(24) Vlasova, N. N.; Pozhidaev, Y. N.; Raspopina, O. Y.; Belousova, L. I.; Voronkov, M. G. *Russ. J. Gen. Chem.* **1999**, *69*, 1391−4.
(25) Brinker, C. J.; Sehgal, R.; Hietala, S. L.; Deshpande, R.; Smith, D. M.; Loy, D.; Ashley, C. S. *J. Membr. Sci.* **1994**, *94*, 85−102.
(26) Choi, K. M.; Shea, K. J. In *Photonic Polymer Synthesis*; Wise, G. W., Trantolo, M., Graham, B., Eds.; Marcel Dekker: New York, 1998; pp 437−80.
(27) Schaefer, D. W. *Science* **1989**, *243*, 1023.
(28) Schaefer, D. W.; Keefer, K. D. In *Better Ceramics Through Chemistry II*; Brinker, C. J., Clark, D. E., Ulrich, D. R., Eds.; Mater. Res. Soc. Symp. Proc. 73; Materials Research Society: Pittsburgh, PA, 1987; p 277.
(29) Schaefer, D. W. *MRS Bul.* **1988**, *13*, 22−7.
(30) Schaefer, D. W.; Beaucage, G. B.; Loy, D. A.; Ulibarri, T. A.; Black, E.; Shea, K. J.; Buss, R. J. In *Better Ceramics through Chemistry VII: Organic/Inorganic Hybrid Materials*; Coltrain, B. K., Sanchez, C., Schaefer, D. W., Wilkes, G., Eds.; Mater. Res. Soc. Symp. Proc. 435; Materials Research Society: Pittsburgh, PA, 1996; pp 301−5.
(31) Boury, B.; Chevalier, P.; Corriu, R. J. P.; Delord, P.; Moreau, J. J. E.; Chiman, M. W. *Chem. Mater.* **1999**, *11*, 281−91.
(32) Chevalier, P.; Corriu, R. J. P.; Delord, P.; Moreau, J. J. E.; Man, M. W. C. *New J. Chem.* **1998**, *22*, 423−33.

These results show extreme sensitivity of the texture to synthetic variables such as bridging group,[4,15,16,33] catalyst,[34,35] temperature,[36] solvent[11] and drying protocol[3,37] and aging.[38] Cerveau et al. legitimately associated this sensitivity to the fact that these materials are synthesized far-from-equilibrium.[11,17] Kinetically controlled systems often display fractal morphologies,[27,29] which we also observe for the aryl-bridged systems studied here. Our contention, however, is that although kinetic factors control short-scale surface texture, thermodynamic factors dominate larger-scale pore formation and may lead to previously unappreciated systematics. Hopefully our taxonomy will aid researchers in systematically controlling porosity with precursor chemistry.

Morphology of Porous Solids

Small-Angle Scattering. Small-angle scattering (SAS) is a powerful technique for characterizing materials in the 5−500 Å size regime.[39] One measures the scattered intensity, I, vs scattering angle, θ, and intensity profiles are routinely plotted versus the scattering vector, q, which is related to θ by the following equation that looks suspiciously like Bragg's Law:

$$q = (4\pi/\lambda) \sin(\theta/2) = 2\pi/L, \qquad (1)$$

where λ is the wavelength of the radiation in the medium. The scattering vector, q, has the units of reciprocal length and is the spatial Fourier frequency of the contrast fluctuations giving rise to the scattering. Typical small-angle X-ray and neutron scattering instruments cover the range $0.005\ \text{Å}^{-1} < q < 0.5\ \text{Å}^{-1}$, corresponding to length scales, L, from 1250 Å at $q = 0.005\ \text{Å}^{-1}$ to 12.5 Å at $q = 0.5\ \text{Å}^{-1}$.

Guinier first observed that the correlation range for dilute particles was simply the average particle radius-of-gyration.[40] The Guinier radius, R_G, is extracted from the initial curvature of the scattering profile

$$I(q) = \text{constant} \times \left(1 - \frac{q^2 {R_G}^2}{3} + \cdots\right). \qquad (2)$$

Hence, scattering in this low-q regime is called "Guinier scattering." At low porosity levels, this so-called Guinier correlation length measures the mean pore size (pore chord), whereas it tracks the solid chord at high porosity.[41] To understand the meaning of R_G in porous solids, it is necessary to discuss chord analysis.[42]

Porous solids can be characterized in a general way using chord analysis.[43−45] To define the chords, imagine a test line penetrating a porous solid. The pore chord, d_p, and solid chord, d_s, are defined as the average lengths of intersection of the test line with the open and solid phases. The average distance, d, between solid phases is by definition the sum of the pore and solid chords, $d = d_s + d_p$. We refer to d as the "sum chord."

Given a model for the pore structure, the Guinier radius can be related to these chords. For domains that are randomly interdispersed, for example, Debye, Anderson, and Brumberger[46] show that the spatial density correlations decay exponentially with a correlation range, a, that is equal to the harmonic-mean of the pore and solid chords.[41]

$$a = \frac{d_s d_p}{d_s + d_p} = \varphi_s(1 - \varphi_s)d = (1 - \varphi_s)d_s \qquad (3)$$

where φ_s is the volume fraction of the solid phase. For this case, fitting the resulting Debye-Anderson-Brumberger scattering function[46] to eq 2 shows that

$$R_G = \sqrt{6}a = \sqrt{6}(1 - \varphi_s)d_s \qquad (4)$$

Note that for a low-density solid $\varphi_s \ll 1$ so

$$R_G \cong \sqrt{6}d_s \qquad (5)$$

That is, the measured Guinier radius is proportional to the solid chord, not to the pore chord. To first approximation, therefore, R_G is simply the strut size.

Equation 4 can be compared to the result for a collection of dilute spheres of radius R.[40] In this case

$$R_G = \sqrt{\frac{3}{5}}R = \sqrt{\frac{27}{80}}d_s \qquad (6)$$

For a sphere, $d_s = 4R/3$, from pure geometry. In principle, d_s can also be obtained from the BET surface area (see below), so these equations will be useful to compare the results of the two characterization methods.

Often, Guinier scattering is followed by a region of power-law scattering. When one is fortunate enough to observe power-law scattering ($I \approx q^{-P}$), interpretation of scattering profiles can be quite simple[28,29,47−49] based on the magnitude of the power-law exponent, P. Porod,[50] and van Nordstrand and Hach[51] showed that for a sharp, smooth interface, $P = 4$. The relationship $I(q) \approx$

(33) Ben, F.; Boury, B.; Corriu, R. J. P.; Le Strat, V. *Chem. Mater.* **2000**, *12*, 3249−52.
(34) Baugher, B. M.; Schneider, D. A.; Loy, D. A.; Rahimian, K. In *Organic/Inorganic Hybrid Materials II*; Klein, L. C., Francis, L., DeGuire, M. R., Mark, J. E., Eds.; Mater. Res. Soc. Symp. Proc. 576; Materials Research Society: Pittsburgh, PA, 1999; pp 105−10.
(35) Cerveau, G.; Corriu, R. J. P.; Framery, E. *Polyhedron* **2000**, *19*, 307−13.
(36) Cerveau, G. A.; Corriu, R. J. P.; Framery, E. *J. Mater. Chem.* **2000**, *10*, 1617−22.
(37) Loy, D. A.; Jamison, G. M.; Baugher, B. M.; Myers, S. A.; Assink, R. A.; Shea, K. J. *Chem. Mater.* **1996**, *8*, 656−63.
(38) Cerveau, G.; Corriu, R. J. P.; Framery, E. *J. Mater. Chem.* **2001**, *11*, 713−7.
(39) Roe, R.-J. *Methods of X-ray and Neutron Scattering in Polymer Science*; Oxford University Press: New York, 2000.
(40) Guinier, A.; Fournet, G. *Small-Angle Scattering of X-rays*; John Wiley and Sons: New York, 1955.
(41) Fernandez, A. M.; Wignall, G. D.; Sperling, L. H. In *Multicomponent Polymer Materials*; Paul, D. R., Sperling, L. H., Eds.; Advances in Chemistry Series 211; American Chemical Society: Washington, DC, 1986; pp 153−70.
(42) Kratky, O. *Pure Appl. Chem.* **1966**, *12*.
(43) Underwood, E. E. *Quantitative Stereology*; Addison-Wesley Publishing Company: Reading, MA, 1970.
(44) Aubert, J. H. *Cellular Plastics* **1988**, *24*, 132−45.
(45) Schaefer, D. W.; Brow, R. K.; Olivier, B. J.; Rieker, T.; Beaucage, G. B.; Hrubesh, L. R.; Lin, J. S. In *Advances in Small-Angle Scattering*; Brumberger, H., Ed.; Kluwer Academic: Boston, 1994; pp 299−307.
(46) Debye, P.; Anderson, H. R.; Brumberger, H. *J. Appl. Phys.* **1958**, *28*, 579.
(47) Martin, J. E.; Hurd, A. J. *J. Appl. Crystallogr.* **1987**, *20*, 61−78.
(48) Schaefer, D. W.; Bunker, B. C.; Wilcoxon, J. P. *Proc. R. Soc. London A* **1989**, *423*, 35−53.
(49) Schmidt, P. W. In *The Fractal Approach to Heterogeneous Chemistry: Surfaces, Colloids and Polymers*; Avnir, D., Ed.; John Wiley & Sons: New York, 1989; pp 67−78.
(50) Porod, G. *Kölloid-Z* **1951**, *124*, 83.

q^{-4} is called Porod's law. Bale and Schmidt[52] later concluded that deviations from $P = 4$ are expected for rough interfaces, but the profile remains power-law for self-similar (or self-affine) fractal interfaces with $3 < P < 4$. As P increases from 3 to 4 the surface becomes increasingly smooth. The roughness is characterized by a surface fractal dimension, $D_s = 6 - P$. A smooth surface is a two-dimensional object so $D_s = 2$. D_s cannot be larger than three, which is the dimension of the most jagged surface that will fit in a three-dimensional embedding space. The important point is that when exponents between 3 and 4 are observed, the surface is rough and its surface dimension is greater than 2, but less than 3. In this case the surface area is ill-defined in that it depends on the measurement length scale.[53,54] Because we do observe such exponents in porous solids derived from bridged silsesquioxanes, this ambiguity may account for the high variability of BET-derived surface areas.

Attempts to increase the roughness beyond $D_s = 3$ destroy the surface completely, leading to a "mass fractal." Mass fractals are best thought of as irregular networks and give scattering exponents $1 < P < 3$.[47] In this case $P = D$, where D with no subscript is the mass-fractal dimension. The limits 1 and 3 correspond to a rod ($D = 1$) and uniformly dense object ($D = 3$). A thin disk, a random-walk polymer, and perhaps other objects give a dimension of $D = 2$, so there is no unique relationship between dimension and morphology. A typical branched polymer has $D = 2.5$. The case $P = 3$ corresponds to the crossover from a mass to a surface fractal.

BET Surface Areas. Internal surface area measured by gas adsorption is a common parameter used to characterize porosity. Others and we have applied this method to the study of bridged silsesquioxanes. Surface area is usually determined by the Brunauer–Emmett–Teller (BET) gas-adsorption method. The BET method probes only the "open" porosity accessible to nitrogen. Scattering, on the other hand, arises from interfaces regardless of the connectedness of the pores, thus providing a measure of the total surface area.

To compare morphological data from BET and SAS, it is necessary to relate the surface area to the chords described above. The relationship among the sum chord, d, solid chord, d_s, and the surface area is simple.

$$d = \frac{4}{S_v} = \frac{4}{\rho S_m} \tag{7}$$

$$d_s = \varphi_s d = \frac{4}{\rho_s S_m} \tag{8}$$

where S_v is the surface area per unit volume, S_m is the surface area per unit mass, ρ is the sample density, and ρ_s is the solid phase or skeletal density.

Equation 7 is readily derived by considering the intersection of the previously described test line with the internal surfaces. Following Underwood,[43] the probability, P_a, that a test line will intersect an element, $\triangle S$, of solid (strut) surface is equal to the projection of $\triangle S$ on a plane normal to the test line, divided by the total area, L^2. That is, $P_a = (\triangle S \cos\theta)/L^2$ where θ is the angle between the probe line and the surface element, and L is the dimension of the sample. Dividing by the length of the test line (L), summing over all surface elements, and averaging θ angle gives the total probability, P_l, per unit length that the line intersects a pore surface: $P_l = S_v/2$. P_l is also related to d as $P_l = 2/d$ where the factor of 2 arises because the domains are bounded by two surfaces. Combining these two relationships for P_l leads to the fundamental result, $d = 4/S_v$. This so-called Cauchy equation has been derived by many investigators in many different contexts. Eq 8 will prove useful when we compare morphological information from BET with that derived from SAS. Eq 8 shows that the BET surface area is a measure of the strut size (d_s), not the pore size (d_p). Of course if the density of the sample is known, one can be derived from the other, as d in eq 7 is equal to $d_s + d_p$.

Equations 7 and 8 assume smooth interfaces. In this case, the d_s derived from BET should agree with that derived from eqs 2 and 5 using SAS data. For rough surfaces, however, the surface area is ill defined and one expects BET to yield a larger S_v than SAS because BET probes length scales of the order of 2 Å, whereas SAS probes length scales greater than 10 Å.

Pore size distributions obtained from gas absorption (capillary condensation) are also complementary to morphological data from SAS. In both cases, models are required to invert the data. For strut-like morphology of silicate aerogels and xerogels, however, standard models used by gas-adsorption equipment manufacturers may not be realistic. SAS also depends on models, but some features such as the Guinier radius are, to first approximation, independent of models.

Experimental Section

Synthesis of Xerogels (X). Xerogels (**X-1** through **X-4**) were prepared by polymerizing monomers **1**–**4** (0.2 M) in tetrahydrofuran (THF) with water.[15] Acid-catalyzed polymerizations were performed using six equiv of water and hydrochloric acid as catalyst (0.022 M HCl in polymerization solution, 10.8 mol % relative to monomer concentration). After gelation, the gels were allowed to age for 48 h before solvent processing and drying. Solvent processing involved exchanging out THF with solvents of progressively decreasing dielectrics until the gel was saturated in 1,1,2-trichloro-1,2,2-trifluoroethane.[15] The resulting gels were air-dried for 18–24 h, ground with a mortar and pestle, and then dried under vacuum for 24 h. Base-catalyzed polymerizations were carried out using ammonium hydroxide (1.14 M NH_4OH or 570 mol %) followed by the gel aging and processing protocol described above.

Synthesis of Aerogels (A). Aerogels (**A-1** and **A-2**) were prepared from monomers **1** and **2** (0.4 M in THF) with three equiv of water under acid-catalyzed (HCl) and base-catalyzed (NH_4OH) polymerization conditions. Sol–gel polymerizations of **1** were performed with varying catalyst concentrations. Acid-catalyzed polymerizations were performed with 4.3×10^{-2} M HCl (10.8 mol %) as catalyst. Gels were formed for the 10.8 mol % HCl. Base-catalyzed polymerizations were performed at 2.2×10^{-4} M NH_4OH (0.054 mol % relative to monomer), 2.2×10^{-3} M NH_4OH (0.54 mol %), 2.2×10^{-2} M NH_4OH (5.4 mol %), 2.2×10^{-1} M NH_4OH (54 mol %), and 2.2 M NH_4OH (540 mol %). Gels were formed for 0.54, 5.4, 54, and 540 mol

(51) Van Nordstrand, R. A.; Hach, K. M. *Small-Angle X-ray Scattering of Silica and Alumina Gels*. Proceedings of the American Chemical Society Meeting, Chicago, 1953; pp 61–8.
(52) Bale, H. D.; Schmidt, P. W. *Phys. Rev. Lett.* **1984**, *53*, 596–9.
(53) Avnir, D.; Farin, D.; Pfeifer, P. *J. Chem. Phys.* **1983**, *79*, 3566–71.
(54) Avnir, D.; Farin, D.; Pfeifer, P. *New J. Chem.* **1992**, *16*, 439–49.

% NH_4OH. To prepare aerogels, the THF was exchanged for methanol before supercritical extraction and drying with carbon dioxide at 1400 psi and 35 °C.[3]

Small-Angle Scattering. Small-angle neutron scattering (SANS) experiments were carried out using the Low-q Diffractometer (LQD) at the Manuel Lujan Neutron Scattering Center at Los Alamos National Laboratory and 30-m SANS camera at the High Flux Isotope Reactor at Oak Ridge National Laboratory (ORNL). Small-angle X-ray scattering (SAXS) experiments were accomplished at ORNL's 10-meter SAXS facility.[55] These data were supplemented with ultra small-angle measurements (USAXS) on the NIST Bonse-Hart X-ray camera,[56,57] which, at the time the experiments were performed, was located on the ×23A beam line at the National Synchrotron Light Source at Brookhaven National Laboratory. The Bonse-Hart data were desmeared, and profiles for different q ranges were matched by an arbitrary vertical shift factor.

Some of the data were measured on an absolute scale. To obtain absolute data, we performed neutron scattering on powders of known density by filling standard spectrophotometer cuvettes and weighing them. Because of the presence of incoherent background scattering from protons, however, neutron scattering did not give measurable signal-above-background for $q > 0.15$ Å^{-1}. To obtain data in this regime we used SAXS, but were not able to obtain absolute data because of the very thin samples required. Fortunately, the SAXS and SANS data show the same scattering profile in the region of overlap, allowing us to extend the absolute SANS data by patching on the SAXS data. At small angles, where the coherent scattering arises from contrast between solid and pore, this procedure is legitimate.

Surface Area and Porosity Characterization.[58] Nitrogen and argon sorption measurements were obtained on a Micromeritics ASAP 2000 at 77 and 87 K, respectively. Specific surface areas were calculated using the Brunauer−Emmett−Teller (BET) theory[59] with multipoint data acquisition. Nitrogen pore size distribution profiles were calculated using the Kelvin equation[60] and the Barrett−Joyner−Halenda (BJH) theory[61] assuming cylindrical pores. Argon pore size distribution profiles were calculated using the Horvath−Kawasoe theory[62] assuming slit-shaped pores. All samples were dried at 100 °C for at least 8 h prior to analysis and were not sized prior to analysis.

Results and Discussion

Arylene-Bridged Polysilsesquioxane Xerogels. Small-angle scattering profiles for a series of arylene-bridged polysilsesquioxane xerogels with 1,3,5-phenylene (**X-4**), 1,4-phenylene **(X-1**), and 4,4′-biphenylene (**X-2**) bridging groups are displayed in Figures 2 and 3. These data represent a composite of X-ray and neutron measurements on powders. In Figure 2, data are plotted as absolute neutron differential scattering cross section per unit sample mass. These data, along with X-ray scattering data for the 4,4′-terphenylene-bridged polysilsesquioxane xerogels (**X-3**), are displayed in Figure 3, but shifted relative to one another. For Figure 2, intense ultra small-angle scattering at small q has been subtracted. Below we show that this scattering arises from the drying process; we attribute it to microcracking caused by strong surface-tension-driven compressive forces active during solvent evaporation.[63]

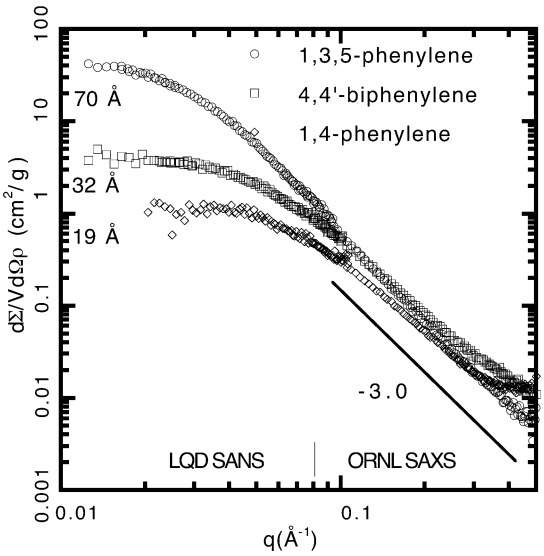

Figure 2. Combined X-ray and neutron data for arylene-bridged polysilsesquioxane xerogels. Small-q scattering arising from xerogel grain structure has been subtracted. The data show increasing correlation range (Guinier radius) with decreasing organic content. The Guinier radius is shown for each curve. The 70 Å correlation range for the upper curve is similar to that of xerogels derived from the sol−gel polymerization of tetralkoxysilanes. The data are presented as the neutron differential scattering cross-section per unit sample mass. Power-law scattering at low q arising from large structures has been subtracted from the data. See Figure 3 for the unsubtracted analogues.

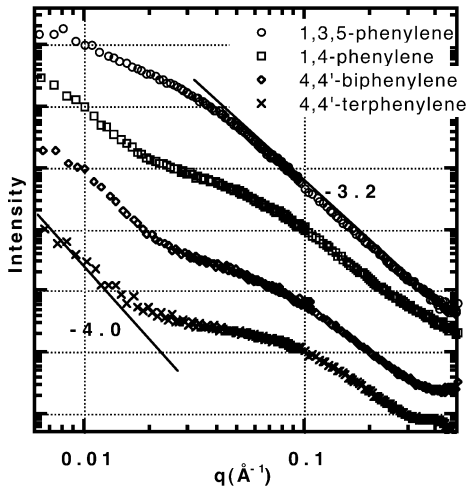

Figure 3. Offset scattering data for arylene-bridged polysilsesquioxane xerogels. The data are shifted vertically by an arbitrary amount to reveal the details of the scattering curves. The less interesting small-q data, subtracted in Figure 2, are included here. The limiting slope of −3.2 for the 1,3,5 system is indicative of rough interfaces. The Porod regime of the other curves is too small to extract reliably a Porod slope. The same is true for the small-q regime where a line of slope −4.0 is plotted.

(55) Hendricks, R. W. *J. Appl. Crystallogr.* **1978**, *11*, 15−30.
(56) Long, G. G.; Krueger, S. *J. Appl. Crystallogr.* **1989**, *22*, 539−45.
(57) Long, G. G.; Krueger, S.; Jemian, P. R.; Black, D. R.; Burdette, H. E.; Cline, J. P.; Gerhardt, R. A. *J. Appl. Crystallogr.* **1990**, *23*, 535−44.
(58) Gregg, S. J.; Sing, K. S. W. *Adsorption, Surface Area and Porosity*; Academic Press: London, 1982.
(59) Brunnauer, S.; Emmett, P. H.; Teller, E. *J. Am. Chem. Soc.* **1938**, *60*, 309.
(60) Thomson, W. T. *Philos. Mag.* **1871**, *42*, 448.
(61) Barret, E. P.; Joyner, L. G.; Halenda, P. H. *J. Am.n Chem. Soc.* **1951**, *73*, 309.
(62) Horvath, G.; Kawazoe, K. *J. Chem. Eng. Japan* **1983**, *16*, 470−5.
(63) Schaefer, D. W.; Olivier, B. J.; Ashley, C.; Beaucage, G.; Richter, D.; Farago, B.; Frick, B.; Fischer, D. A. *J. Non-Cryst. Solids* **1994**, *172*, 647−55.

To interpret the curves in Figures 2 and 3, we start from comparison to the better-understood tetraalkoxy analogues such as tetraethoxy or tetramethoxy silane (TEOS or TMOS) polymerized under similar conditions.[64−66] Because monomer **4** is the most similar (lowest organic content) to the alkoxy monomers, we take the similarity of the scattering profile for **X-4** to that for published silica xerogels prepared from tetraalkoxysilanes as evidence that the scattering is of similar origin. That is, we interpret the scattering as arising from the pore−solid interface, not from domains resulting from organic−inorganic phase separation. Given the small bridge size and high cross-link density, the bridged systems cannot accommodate segregation into 70-Å organic-rich domains. We presume also there is no disruption of any Si−C bonds. The absence of Q peaks in the solid-state silicon-29 NMR speaks to the stability of the Si−C bond in these materials.[15] Rather, phase separation is the result of topological fluctuations that occur during the solution polymerization. Regions of high cross-link density become incompatible with the solvent and would precipitate were they not linked into the gel network. The network elasticity restricts phase separation of nanometer-length scales.

When compared to silica gels prepared from tetraalkoxysilanes, scattering from **X-4** is very similar in the Guinier regime, where the Guinier radius of 70 Å is calculated, but displays a measurably smaller slope at large q. That is, most alkoxysilane-based xerogels and, incidentally, alkyl-bridged silsesquioxane based xerogels (not shown), show a limiting slope of -4 at large q, indicative of a smooth pore surface. The novel feature of the aryl-modified material is the absence, at large q, of Porod scattering (slope $= -4.0$) from smooth interfaces. The presence of the organic bridging groups must disrupt the otherwise smooth interface seen in base-catalyzed tetralkoxysilane−silica systems, leading to a rough interface characterized by $D_s \approx 2.8$. For **X-1** − **X-4**, size scale of the porosity is so small (10−32 Å) that the extent of the power-law scattering is too limited to unequivocally extract a slope (see below).

Keefer and Schaefer[67] observed fractally rough porosity in xerogels prepared from partially hydrolyzed TMOS. They attributed the observed roughness to site blocking by unhydrolyzed methoxy groups and proposed a "poisoned Eden model" to explain the roughness. Although the bridging group also acts to block one site on each monomer, fractal roughness is not found within the poisoned Eden model when every monomer has the same functionality. Polymerization of fully hydrolyzed trifunctional monomers simply leads to a less dense, uniform solid phase with asymptotically smooth interfaces.[68] Our results indicate a more disrupted growth process. The bulky aromatic groups might interfere with the silanol condensation, precluding polymerization opportunities as effectively as site-blocking in the Keefer simulations.[68] Indeed, solid state ^{29}Si NMR data indicate that there is a lower degree of condensation in the bridged polysilsesquioxanes compared to that in silica gels prepared under comparable conditions from tetraalkoxysilanes.[69] Short-scale roughness could also be caused by the tendency of the bridging groups to cluster,[70] thereby imposing a crumpled morphology on the surface.

With increasing length of the organic bridging group (**X-3** > **X-2** > **X-1**), the observed Guinier radius (determined from the initial curvature of the data in Figure 2, using eq 2) monotonically decreases compared to that of the 1,3,5-bridged xerogel (**X-4**). This trend can be seen as the migration of the "knee" of the curve in the region 0.02−0.06 Å^{-1} (from 20 to 70 Å) in Figure 2. The monomers with longer bridging groups yield xerogels with smaller domain sizes. Although the increased flexibility imparted by the longer organic bridging groups may accommodate a smaller radius of curvature of the solid phase, we attribute the trend to increasing hydrophobicity, which alters the thermodynamics of phase separation (see Conclusion). As the correlation range decreases, the domain of power-law scattering also decreases, compromising any attempt to extract a meaningful surface fractal dimension except for the 1,3,5-phenylene-bridged polysilsesquioxane xerogels (**X-4**). There is no reason to believe, however, that D_s differs from the ∼2.8 observed for the 1,3,5-phenylene xerogel.

Near $q = 0.4$ Å^{-1}, a faint maximum is observed in the 4,4′-terphenylene-bridged xerogel. This shoulder corresponds to a Bragg spacing of about 15 Å, somewhat larger than the size of the spacer. For smaller spacers, the peak moves out of the experimental window, but the upturn in the 4,4′-biphenylene sample is suggestive of a peak in that sample as well. These results are similar to the observations of Boury, Corriu, and Muramatsu who account for the peak position based on local organization of the bridging groups.[70]

Arylene-Bridged Polysilsesquioxane Aerogels. Evidence for collapse of the gel network during drying comes from comparison of xerogels with identical samples dried supercritically to produce "aerogels." The latter process involves solvent exchange for liquid CO_2 and extraction above the critical temperature of CO_2. Unlike xerogels, which undergo considerable shrinkage (∼85% volume loss) during air-drying, aerogels are thought to preserve more of the original wet-gel structure. Because there is no liquid−gas interface above the critical point, critical drying avoids surface-tension-induced collapse. Figure 4 shows the dependence of the scattering on drying technique for the phenylene-bridged sample. The xerogel curve includes the small-q scattering that had been subtracted in Figure 2. These small-q data were obtained using the Bonse-Hart USAXS system at NSLS.

Two features of Figure 4 are apparent. First of all, the Guinier crossover lies at $q \approx 0.01$ Å^{-1} in the aerogel, whereas it is observed at $q \approx 0.03$ Å^{-1} in the xerogel. This shift implies a smaller Guinier correlation length,

(64) Schaefer, D. W. *J. Phys.-Colloque* **1988**, *24-C4*, 121−6.
(65) Schaefer, D. W.; Brinker, C. J.; Wilcoxon, J. P.; Wu, D. Q.; Phillips, J. C.; Chu, B. In *Better Ceramics Through Chemistry III*; Brinker, C. J., Clark, D. E., Ulrich, D. R., Eds.; Mater. Res. Soc. Symp. Proc. 121; Materials Research Society: Pittsburgh, PA, 1988; pp 691−6.
(66) Schaefer, D. W. *MRS Bull.* **1994**, *24*, 49−53.
(67) Schaefer, D. W.; Keefer, K. D. *Phys. Rev. Lett.* **1986**, *56*, 2199−202.
(68) Keefer, K. D. In *Better Ceramics Through Chemistry II*; Brinker, C. J., Clark, D. E., Ulrich, D. R., Eds.; Mater. Res. Soc. Symp. Proc. 121; Materials Research Society: Pittsburgh, PA, 1986; pp 295−304.
(69) Brinker, C. J.; Scherer, G. W. *Sol−Gel Science: The Physics and Chemistry of Sol−Gel Processing*; Academic Press: Boston, 1990.
(70) Boury, B.; Corriu, R. J. P.; Delord, P.; Le Strat, V. *J. Non-Cryst. Solids* **2000**, *265*, 41−50.

Table 1. Synthetic Conditions and BET Surface Areas for Samples Used

Figure	bridge	form	monomer concn [M]	H_20/Si	catalyst	catalyst concn[a]	solvent	N_2 [b] m^2/g	density g/cm^3
2,3,4	1,4-phenylene	xerogel	0.2	3	HCl	10.8	THF	958	0.64
5	1,4-phenylene	aerogel	0.4	1.5	HCl	10.8	THF	962	0.27
4,5	1,4-phenylene	aerogel	0.4	1.5	NH_3	540	THF	1670	0.08
6,7	1,4-phenylene	aerogel	0.4	1.5	NH_3	54	THF		0.19
6,7	1,4-phenylene	aerogel	0.4	1.5	NH_3	5.4	THF		0.37
6	1,4-phenylene	aerogel	0.4	1.5	NH_3	0.54	THF		0.36
2,3	4,4′-biphenylene	xerogel	0.2	3	HCl	10.8	THF		0.71
3	4,4″-terphenylene	xerogel	0.2	3	HCl	10.8	THF		
2,3	1,3,5-phenylene	xerogel	0.2	3	HCl	10.8	THF	756	0.28

[a] Mol % = 100 × [catalyst]/[monomer]. [b] Nitrogen BET surface area.

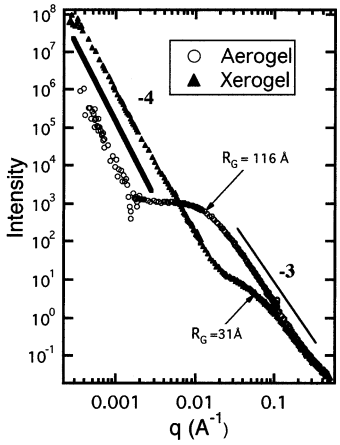

Figure 4. Comparison of scattering profiles for 10.8%-acid-catalyzed aerogel and xerogel derived from 1,4-phenylene-bridged polysilsesquioxanes (**A-1** and **X-1**). The xerogel data were scaled to match the aerogel data at large *q*. The aerogel data are a combination of USAXS and SAXS, and xerogel data are a combination of USAXS and SANS.

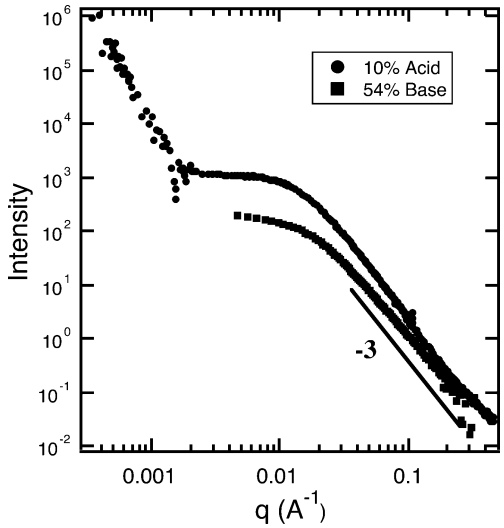

Figure 5. Comparison of acid- and base-catalyzed, 1,4-phenylene-bridged polysilsesquioxanes aerogels. The presence of scattering below 0.001 $Å^{-1}$ for the acid-catalyzed systems indicates that large-scale inhomogeneities develop even during supercritical drying for the acid-catalyzed system. Unfortunately, low-*q* Bonse-Hart data are not available for the base-catalyzed system. Overall, the results are consistent with the acidic system being somewhat more collapsed due to decrease branching during solution polymerization.

as expected for a more collapsed xerogel structure. It is interesting to note that no measurable change in slope is observed in the Porod regime beyond $q = 0.04$ $Å^{-1}$. The strut structure collapses on large scales leaving the surface features unchanged.

The most evident difference between the curves in Figure 4 is the absence of intense scattering at small *q* for the supercritically dried sample. The difference shows that the small-*q* scattering is caused by drying-induced stresses that presumably lead to grains or other large-scale morphological features. The small-*q* scattering follows a −4.0-power-law consistent with sharp grain interfaces on length scales of the order of one micrometer. The size of the morphological features causing this scattering is too large to be resolved by the instrument.

Acid- vs Base-Catalyzed Polysilsesquioxane Aerogels. Phenylene-bridged polysilsesquioxane aerogels (**A-1**) were prepared by both acid- and base-catalyzed sol−gel processing. The molar ratio of catalyst to monomer is given in Table 1. Both aerogels are characterized by nitrogen sorption porosimetry. The acid-catalyzed aerogel had a surface area of 1200 m^2/g and the base-catalyzed aerogel had a surface area (BET) of 1600 m^2/g. From these numbers and eq 8 we calculate a solid chord of 21 Å for the acid-catalyzed system and 17.5 Å for the base-catalyzed system. Then, from eq 4 the predicted Guinier radius is 53 Å for the base-catalyzed and 43 Å for the acid-catalyzed aerogel.

The data in Figure 5 show that the morphologies are very similar in the regime between 20 and 500 Å. A correlation range of 120 Å is found in both cases, substantially larger than that expected on the basis of gas adsorption. On the basis of these numbers it can be said that BET is not sensitive to porosity, but is sensitive to surface texture. The reason is because BET is probing the surface on dimensional scales much smaller than the strut or pore diameter. The limiting slopes in Figure 5 show that the strut surface is very rough ($P \approx 3$) in both cases. In this case surface area depends on probe length, and the BET-derived chords cannot be identified with the strut size found by SAS.

On an absolute scale, the intensity of the base-catalyzed sample in Figure 5 falls below that of the acid-catalyzed analogue, implying smaller strut surface area. This result is unexpected based on the larger BET surface area of the base-catalyzed sample. In addition, the somewhat smaller slope at large *q* for the base-catalyzed systems implies greater surface roughness, which would lead to greater BET surface area. These differences reinforce the need for caution in extracting morphological information from BET surface areas. SAS shows that there are no smooth interfaces in either

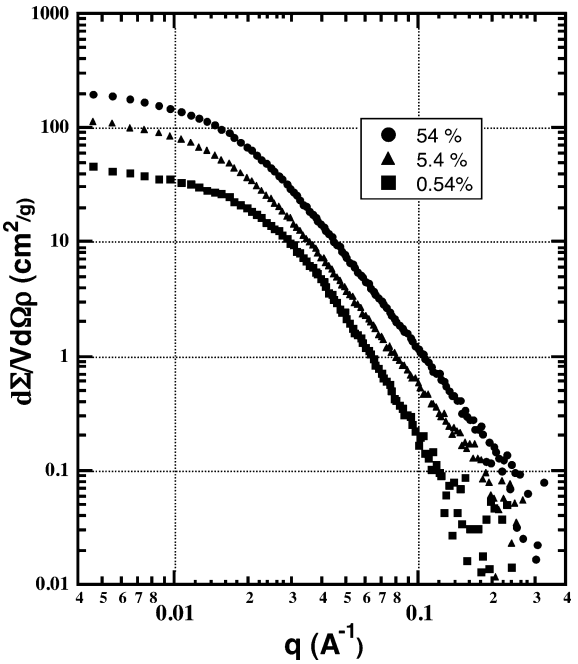

Figure 6. LQD SANS data comparing base-catalyzed 1,4-phenylene-bridged aerogels reacted at differing pH. A flat background was subtracted, compromising the high-q data. Comparison with the SAXS data on the same samples in Figure 7, however, indicates that the limiting slope may be somewhat steeper than −2.7. The 0.54% sample was a powder confined in a cuvette. The other samples were monoliths.

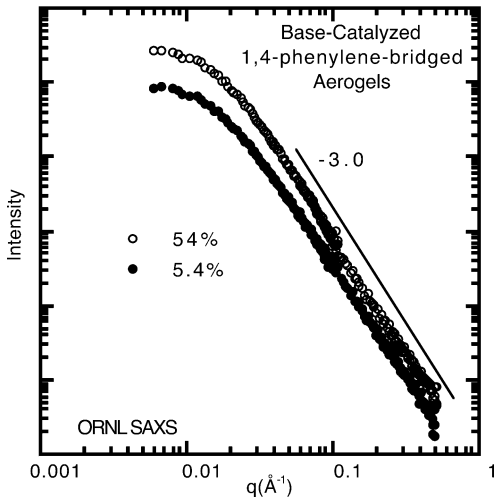

Figure 7. ORNL SAXS data for 1,4-phenylene-bridged aerogels reacted at two base concentrations. The data are not on an absolute scale and can be compared only with regard to shape. The slight increase in slope compared to the SANS data in Figure 6 is probably due to the fact that the SANS data require a background subtraction. The X-ray scattering is so intense that no background is evident even at $q = 0.5$ Å^{-1}.

sample, precluding the existence of a probe-independent "surface area."

Despite ambiguities in interpretation of surface area, it is safe to conclude that the acid-catalyzed and base-catalyzed systems differ only quantitatively. There is no evidence of any fundamental difference in the mechanism of pore formation as a function of catalyst. Overall the SAS data and sample densities in Table 1 are consistent with somewhat greater collapse during supercritical drying for the acid-catalyzed system compared to the base-catalyzed system. This conclusion tracks that in an alkoxy-derived system where the increased branching of the base-catalyzed materials leads to greater local stiffness and increased resistance to drying stresses.

Effect of Catalyst Concentration. In our final experiment, we studied the effect of catalyst concentration on the structure of base-catalyzed 1,4-phenylene-bridged aerogels (**A-1**). We used both LQD SANS and ORNL SAXS. We were able to obtain absolute scattered intensities for the SANS data contained in Figure 6. These data, however, displayed a flat background due to incoherent scattering that had to be subtracted, compromising the high q data. The SAXS data in Figure 7, on the other hand, required no background subtraction. In this case, however, we were unable to obtain absolute intensity data.

The data in Figures 6 and 7 show that there is minimal change in structure above 5.4% catalyst. The 0.54% sample, however, shows measurably less scattering and evidence of mass fractal character. The transition from mass-fractal ($P < 3$) to surface-fractal ($P > 3$) structure is probably due to increased cross-link density for the higher catalyst concentrations. The 0.54% sample lacked integrity and powdered during drying, also indicative of weaker cross-linking. Weaker cross-linking allows domain collapse and a transition from a polymer-like network structure to distinct microphase-separated domains with rough surfaces. The SAXS data in Figure 7 are consistent with these conclusions, but the limiting Porod slopes are steeper (−3.0 vs. −2.7) indicating an object that is near the mass-fractal−surface-fractal crossover. This difference could, in principle, be due to different elemental sensitivities of SAXS and SANS. More likely, the SANS data analysis is compromised by the required background subtraction.

Conclusions

We find no qualitative change in the morphology with bridging group structure (within the aryl family), catalyst type, or catalyst concentration, although we did observe a decrease in the correlation range (roughly the strut size) with increasing organic content. Small-angle scattering reveals that structure in the Porod region ($q \gg 2\pi/R_G$) in arylene-bridged polysilsesquioxanes is nearly unaffected by reaction conditions used in the gel preparation. At larger q, the observed power-law slopes show that the strut interfaces are extremely rough. This roughness has a strong influence on gas adsorption because the probe molecules are comparable to the size-scale of the roughness.

On the basis of the shift in the Guinier radii in Figure 4, aerogels were shown to have average domain sizes greater by a factor of 3 than the corresponding xerogels. Differences in average domain size between the aerogels and xerogels, however, were not accompanied by a significant difference in the fractal properties; both materials displayed Porod slopes of near −3, indicative of a solid right at the crossover from a mass fractal to a surface fractal. The type of catalyst used during the preparation of the gels also had no qualitative effect on the scattering profiles.

Overall, this study shows that pore morphology is weakly dependent on all the variables studied, which

include bridging group, drying protocol, catalyst type, and catalyst concentration. This result seems to contradict other studies, which reveal substantial differences in texture with all these parameters. The discrepancy lies in the fact that gas adsorption is sensitive to short-scale surface roughness, which is much more sensitive to local bonding and synthetic chemistry. The scattering data show that the surfaces are exceedingly rough, and presumably this roughness has a considerable effect on gas adsorption behavior. It must be remembered, however, that these conclusions apply to only aryl-bridged systems. In alkyl-bridged systems we find smooth interfaces (not shown).

We do observe a major change in domain size with bridging group. The higher the organic content, the smaller the domain size. We envision that pore formation is due to nanoscale phase separation that is triggered by cross-linking. As cross-linking proceeds, the growing network polymer becomes increasingly incompatible with the solvent. Because of fluctuations in cross-link density, regions of high cross-link density phase-separate before regions of low cross-link density. The size scale of the resulting domains (ultimately the struts) depends on competing interactions. An enthalpic driving force, controlled by the hydrophobicity of the monomer, favors large-scale phase separation, whereas the entropic contribution due to elasticity favors short-scale phase separation. The ultimate domain size results from a competition between the opposing influences.

The postulated phase separation does not involve segregation of the organic from the inorganic moieties. Rather, highly cross-linked regions expel solvent whereas weakly cross-linked regions remain swollen. In the wet-gel the domains differ in topology, not chemistry.

As the organic content of the monomer increases, the enthalpic contribution to the free energy apparently decreases. That is, the system is more compatible with the solvent and therefore remains swollen further into the cross-linking reaction. When phase separation does ultimately occur, the network is tighter leading to a severe entropic penalty for large-scale phase separation. Thus, aerogels with high organic content remain single-phase longer, but when they do phase-separate, the domains are necessarily small. In this model, a combination of kinetic and thermodynamic factors controls the morphology.

The above analysis should apply regardless of the details of the synthetic protocol, thus explaining the weak dependence of morphology on most processing variables. Texture, however, as measured by gas adsorption, is very sensitive to short-scale chemical structure and therefore is much more sensitive to kinetic factors that control bonding. This situation highlights the need to examine these complex materials using both gas adsorption and scattering.

Acknowledgment. Part of this work was performed at the facilities of Oak Ridge, Los Alamos, and Brookhaven National Laboratories. We thank George Wignall and Phil Seager for supervision of data collection at these facilities. USAX work was done using the NIST USAXS camera, which at the time of the experiment was located at the X-23A3 beam line (supported by the U.S. Department of Commerce) at the National Synchrotron Light Source (NSLS) at Brookhaven National Laboratory. The NSLS is supported by the U.S. Department of Energy, Division of Materials Sciences and Division of Chemical Sciences, under Contract DE-AC02-98CH10886. We thank Daniel A. Fischer for his assistance in collection of the USAXS data. This work benefited from the use of the Low-*q* Diffractometer at the Manuel Lujan Neutron Scattering Center of the Los Alamos National Laboratory, which is supported by the Office of Basic Energy Sciences of the United States Department of Energy under contract W-7405-ENG-36 to the University of California. The research at Oak Ridge was sponsored in part by the U. S. Department of Energy under Contract DE-AC05-00OR22725 with the Oak Ridge National Laboratory, managed by UT-Battelle, LLC.

CM0350683